DINAME 2017 - Proceedings of the XVII International Symposium on Dynamic Problems of Mechanics
A. T. Fleury, D. A. Rade, P. R. G. Kurka (Editors), ABCM, São Sebastião, SP, Brazil, March 5-10, 2017

Control of flexible cantilever beams

Leonardo B. Saint Martin[1], **Henrique L. Silveira**[2], **Ricardo U. Mendes**[3], **Katia L. Cavalca**[4]

[1,2,3,4] Department of Integrated Systems, Faculty of Mechanical Engineering, University of Campinas, 200, Mendeleyev street, 13083-860, Campinas, SP, Brazil, [1]leonardo.saintmartin@gmail.com, [2]henriqueleandro82@gmail.com, [3]rumqld@gmail.com, [4]katia@fem.unicamp.br.

Abstract: Electromagnetic actuators are widely used in industrial applications, ranging from exciters (very appropriate when excitation with no contact is required or desired) to more complex applications such as vibration control in mechanisms (such as robotic arms). In the present study, an electromagnetic actuator is used in combination with a PID controller to suppress the vibration of a flexible cantilever metallic beam, in three complementary conditions: natural frequencies of the beam; transient regime; and random excitations. To guarantee the correct tune of the PID controller and consequently the efficiency of the actuator, the two main parameters of the beam (i.e. the Young's modulus of the material and the adequate coefficients for proportional structural damping) were experimentally identified, so that the finite element model was as close as possible to the real dynamic behavior of the cantilever beam. The model adjustment was performed by comparing the frequency response function (FRF) experimentally obtained and the model responses, obtained by numerical simulation. Then, the relay feedback test was applied both to the model and the physical system to determine the ultimate gain and the ultimate frequency of the closed loop systems. From these parameters, five different PID tuning methods were examined in the test rig, being possible to compare their efficiencies both in reducing vibration amplitudes and in conducting the system to its reference position. The adjustments, tuning procedures and tests were repeated considering two different excitation sources: an electromechanic exciter (shaker) and an impact hammer.

Keywords: cantilever beam, vibration, PID controller, electromagnetic actuator.

INTRODUCTION

Magnetic actuators are components with a wide range of possibilities. They may be used in simple applications, like coupling pairs (special rack-and-pinion couplings, for example), to more complex applications, such as Active Magnetic Bearings (AMBs), responsible for levitating and stabilizing rotors during their operation. In fact, the main feature of magnetic actuators is the ability to apply known and controllable forces with no need of contact and no need of any kind of material medium, over many types of elements and structures. Through this mechanism, the application field for these kind of components is growing year after year.

In this paper, it will be presented a special application of magnetic actuators, which consist of its use as a control force source. In other words, a PID controller will act together with an actuator to attenuate the dynamic response (in vibration, flexion modes) of a cantilever beam. The PID controller will be responsible for the quantification of the electromagnetic force (trough some controllable variable, let us say, a current) to be applied on the beam. The actuator will be responsible for converting this control current in effective force, applied to the beam. This special application encounters many correspondents in real applications. It can be used to control excessive movement of flexible robot arms (such as in unmanned, exploration vehicles, including interplanetary purposes) or to stabilize solar panels structures in satellites. Therefore, the objective of this paper is the investigation of an efficient use of a one-direction actuator, together with a PID controller, not just to attenuate both the transient and permanent response of a cantilever beam, but still keep it at some reference position (stabilization).

PROPOSED MODEL AND CALIBRATION

Differential assembly and the electromagnetic force

According to Maslen (2000), the electromagnetic forces provided by the actuators are always attraction forces. Therefore, to be able to obtain a resultant force that could act in both senses of the x-axis, it should be used a pair of actuators positioned one in front of the other, as Fig. 1a illustrates. This characteristic mounting is called *differential assembly*.

In the assembly of the Figs. 1a and 1b, the currents i_1 and i_2 in both coils must be decomposed in two terms: the first, a constant term, equal in both coils, called the bias current, i_b; and the second term, a control current from the PID controller, i_x, which is respectively added and subtracted from each one of the two coils. Is must be remembered that: 1)

the control current must be always smaller or equal to the bias current, because otherwise the resultant currents in the coils would be inverted and this would cause losses by hysteretic effects; and 2) the maximum resultant current must not be high enough so the actuators enter the saturation field.

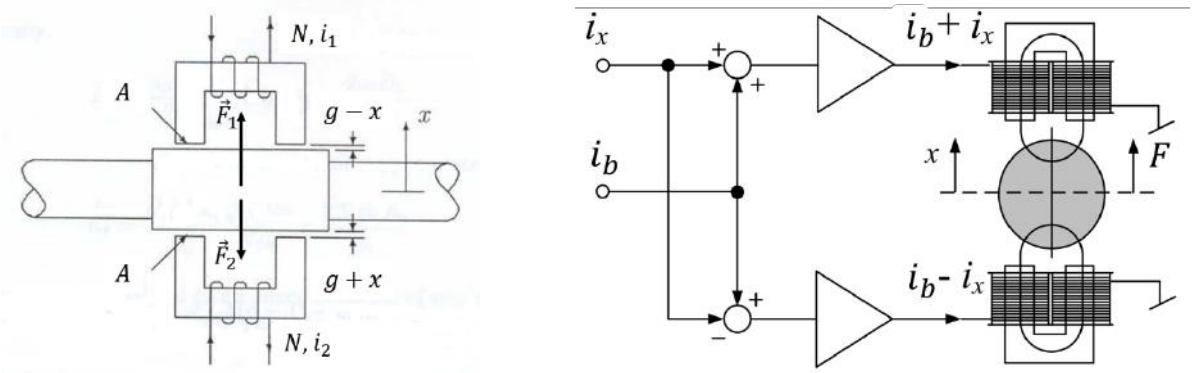

(a) Schematic. **(b) Electrical Connections.**

Figure 1 – Differential assembly of one pair of actuators.

According to Figs. 1a and 1b, the electromagnetic forces F_1 and F_2 and the resultant force F are given by:

$$F_1 = F_{+x} = \varepsilon\mu_0 \frac{N^2 A}{4} \frac{i_1^2}{(g-x)^2} = \varepsilon\mu_0 \frac{N^2 A}{4} \frac{(i_b+i_x)^2}{(g-x)^2} \tag{1a}$$

$$F_2 = F_{-x} = \varepsilon\mu_0 \frac{N^2 A}{4} \frac{i_2^2}{(g+x)^2} = \varepsilon\mu_0 \frac{N^2 A}{4} \frac{(i_b-i_x)^2}{(g+x)^2} \tag{1b}$$

$$F = F_1 - F_2 = \varepsilon\mu_0 \frac{N^2 A}{4} \left[\frac{(i_b+i_x)^2}{(g-x)^2} - \frac{(i_b-i_x)^2}{(g+x)^2}\right] \tag{2}$$

In Eqs. (1)-(2), N is the total number of coils in each actuator; A is the area of the pole (ferromagnetic core) of the actuator; μ_0 is the magnetic permeability of the vacuum (taken for air); and ε is a correction factor due to electromagnetic losses (field lines dispersion) in the air-gap region (adopted value of 0.8). The method of composition of the currents i_1 and i_2 in terms of i_b and i_x intends to let both the actuators work inside their linear region and far enough from the saturation.

By linearizing Eq. (2) around the reference position (half distance from both actuators), where $x = 0$ and the control current, i_x, is also zero (and, therefore, just the bias component remains, $i_1 = i_2 = i_b$), one should obtain Eq. (3).

$$F = \left(\varepsilon\mu_0 \frac{N^2 A}{g^2} i_b\right) i_x + \left(\varepsilon\mu_0 \frac{N^2 A}{g^3} i_b^2\right) x = k_i i_x + k_x x \tag{3}$$

In Eq. (3), k_i and k_x are, respectively, the current stiffness and the position stiffness. Equation (3) allows the calculation of the resultant electromagnetic force when it is known the control current produced by the controller and the position of the beam between the actuators.

Finite Element Model

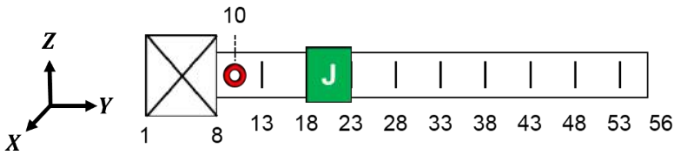

Figure 2 – Finite element model of the cantilever beam.

The cantilever beam was modeled using the finite element method, as show in Fig. 2. The metallic beam (whose dimensions and characteristics are viewed in Tab. 1 and Fig. 3a) was discretized in 55 rectangular elements (56 nodes) of approximately 10 mm length. Each node of the mesh has two degrees of freedom, in the direction of the force provided by the actuator: one translation (x-axis) and one rotation (z-axis). In the position of the actuator, a journal (green square in Fig. 2) was added in order to allow the magnetic flux to circulate on the beam and, consequently, allow the effective application of the magnetic force by the actuator. The dimensions and characteristics of the journal may be viewed in Tab. 2 and in Fig. 3b. The red circle in Fig. 2 denotes the point where the external perturbation was applied, and the first eight nodes represent the part of the beam that was clamped.

Table 1 – Characteristics of the beam.

Parameters	Values
Length (mm)	551 ± 1
Height (mm)	37.8 ±0.1
Thickness (mm)	0.77 ± 0.05
Mass (g)	250.78 ± 0.03
Density (g/cm^3)	6.768 ± 0.002

Table 2 – Dimensions of the journal.

Parameters	Values
Length (mm)	50.28 ± 0.05
Height (mm)	55.23 ±0.05
Outer thickness (mm)	6.50 ± 0.05
Inner thickness (mm)	0.77 ± 0.05

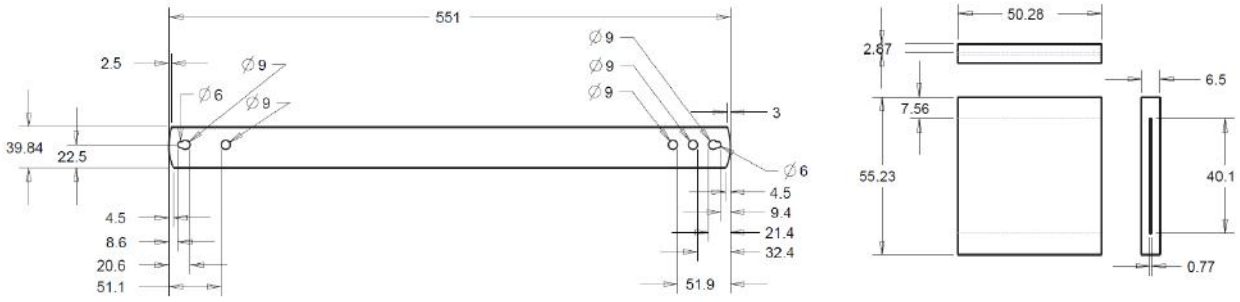

(a) Beam. **(b) Journal.**

Figure 3 – Dimensions (in mm) and characteristics of the beam and the journal.

The composition of mass and stiffness matrices used the Euler-Bernoulli model for beams (as presented by Kwon, 1996), since the small forces applied to the beam resulted in small displacements, allowing the dynamic behavior of the beam to stay within the linear region.

$$\boldsymbol{M_E} = \frac{\rho AL}{420}\begin{bmatrix} 156 & 22L & 54 & -13L \\ 22L & 4L^2 & 13L & -3L^2 \\ 54 & 13L & 156 & -22L \\ -13L & -3L^2 & -22L & 4L^2 \end{bmatrix} \tag{4}$$

$$\boldsymbol{K_E} = \frac{EI_z}{L^3}\begin{bmatrix} 12 & 6L & -12 & 6L \\ 6L & 4L^2 & -6L & 2L^2 \\ -12 & -6L & 12 & -6L \\ 6L & 2L^2 & -6L & 4L^2 \end{bmatrix} \tag{5}$$

In Eqs. (4)-(5), L, A and I_z are, respectively, the length, the transverse area, and the area moment of inertia with respect to the z-axis of the rectangular element in the mesh; ρ is the density of the material of the beam; and E is its Young's modulus.

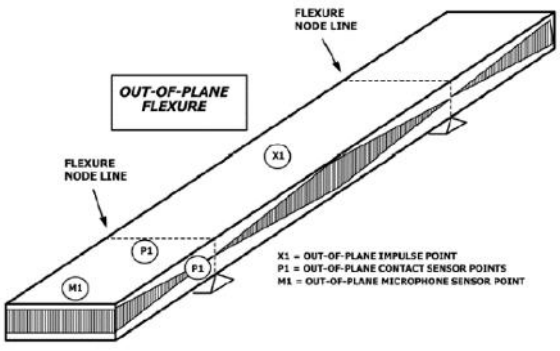

Figure 4 – Supported beam as described in the norm ASTM E 1876-09.

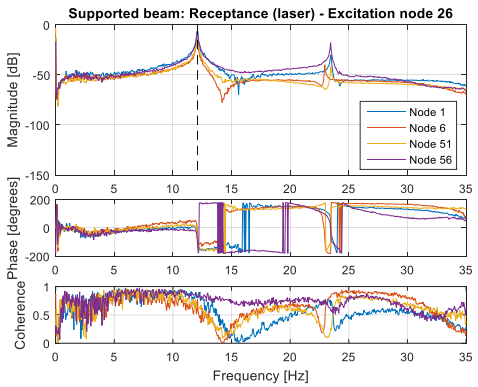

Figure 5 – FRFs in flexion of the supported beam.

Once the analysis proposed in this paper for the beam were dynamic, it should be used the dynamic elastic modulus of the material. This was experimentally obtained, according to the method proposed by the norm ASTM E 1876-09 (2009). According to this norm, the analyzed element must be positioned above two supports as shown in Fig. 4. Then, an impulsive excitation, obtained with an impact hammer with steel tip, should be applied to the center point of the element (X1, Fig. 4). Finally, the dynamic response of the element, in bending, should be measured in points near its extremities (P1 and M1 in Fig. 4, whether the displacement transducer needs or does not need contact).

Figure 5 shows the results obtained for the beam, when applied the test method proposed by the norm and acquired its response, with a laser sensor, at the points M1 and P1, in both its extremities. With the first natural frequency in flexion of the beam, the dynamic Young's modulus of the material could be estimated: E = 138.77 GPa.

For the damping matrix, it was considered the model of proportional structural damping, which predicts that the damping matrix is a linear combination of both the mass and stiffness matrices, through the constants α and β, respectively.

$$\boldsymbol{C_E} = \alpha \boldsymbol{M_E} + \beta \boldsymbol{K_E} \tag{6}$$

However, once the rigid body modes of the beam are irrelevant in this paper (since the focus here is just the bending modes), Maia and Silva (1997) proposes that the mass contribution may be neglected (i.e. $\alpha = 0$). Therefore, the damping matrix is just a weighting of the stiffness matrix.

In practice, β was estimated by comparing the frequency response functions of the empirical modal analysis to those from the correspondent adjusted model. The results for the cantilever beam, with journal coupled, considering: (a) no mass load due to the excitation system (impact hammer) and (b) mass load due to the exciter coupling, are illustrated in Fig. 6. In the specific case of the Fig. 6b, it was necessary to add a mass load in the model node correspondent to the physical position of the exciter in the test rig, once its coupling had changed significantly the dynamic response of the beam. The additional mass load respond for the mass of the stinger and the mass of the load cell, both coupled to the beam when the electromechanic exciter was used.

In Fig. 6, the adjusted value for the coefficient of the proportional damping, β, was 5×10^{-6}.

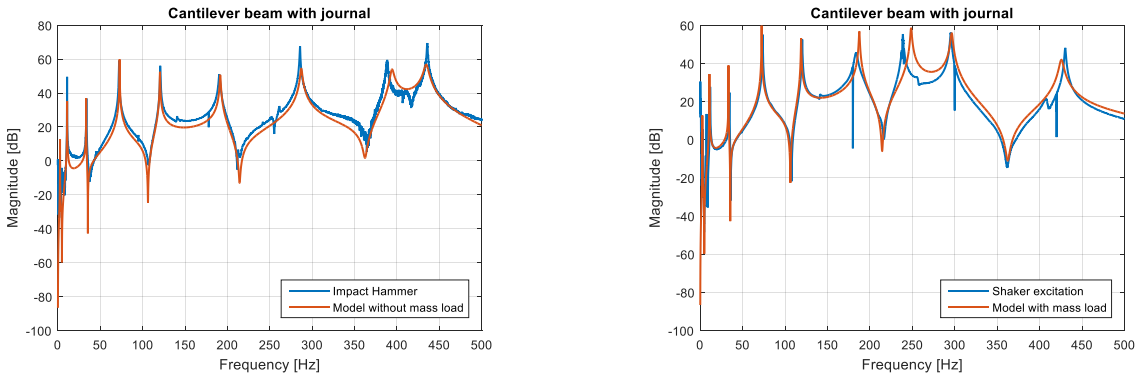

(a) Excitation with impact hammer (node 10). **(b) Excitation with shaker (node 10).**

Figure 6 – Frequency response functions experimentally obtained and from the adjusted complete model.

Model reduction using Guyan's method

Once the step of analyzing the simulated dynamic response of the adjusted system (to tune the PID controller) would require an iterative routine, some model reduction could reduce significantly the computational time effort. Then, it was applied the static reduction as proposed by Guyan (1965, *apud* Friwell *et al*., 2000), since the beam was very flexible and, thus, had very low damping.

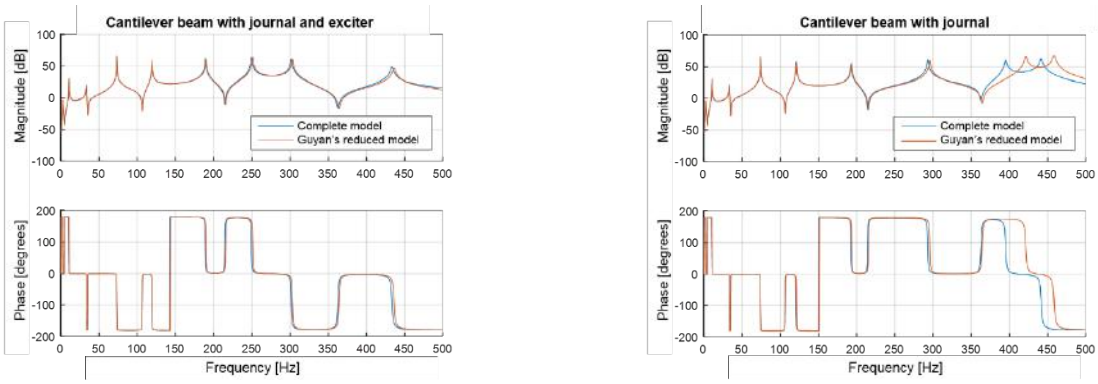

(a) With exciter. **(b) Without exciter.**

Figure 7 – Frequency response functions from the complete model and the reduced model.

During the process of model reduction, some key degrees of freedom were chosen, so it would be possible to reproduce in the reduced model the characteristics and constraints of the correspondent complete model. These degrees of freedom, only in translation, were, mainly: at the edge of the clamped length of the beam, in the node of excitation (external force input), in the transducers nodes, on the journal (electromagnetic force input), and at the points of maximum displacement in the bending modes.

Figure 7 compares both frequency response functions simulated from the complete model and from the reduced model. Once again, the two conditions of excitation were contemplated. The curve fitting can be considered adequated up to 350 Hz, which is fine to the application of this work once the work frequency range is 0 Hz to 100Hz.

Relay feedback test

The adjusted and reduced model was used along with the test scheme proposed by Åström e Hägglund (1994, *apud* Anantachaisilp *et al*., 2012), called the *relay feedback test*, to estimate the parameters for the PID controller tuning. This system was composed by the plant (which means the beam, the displacement sensor, the current amplifier and the actuators) and by a relay instead of the controller. The relay is fed with the negative of the displacement sensor signal and feeds the current amplifier with a fixed voltage that has the same signal of its input, as schematically shown in Fig. 8. The *relay feedback test* is a frequency response method, used to obtain the dynamic information about the system over which the controller would be applied, that has considerable advantage: it is suitable either to a computer model simulation, or to an experimental test rig.

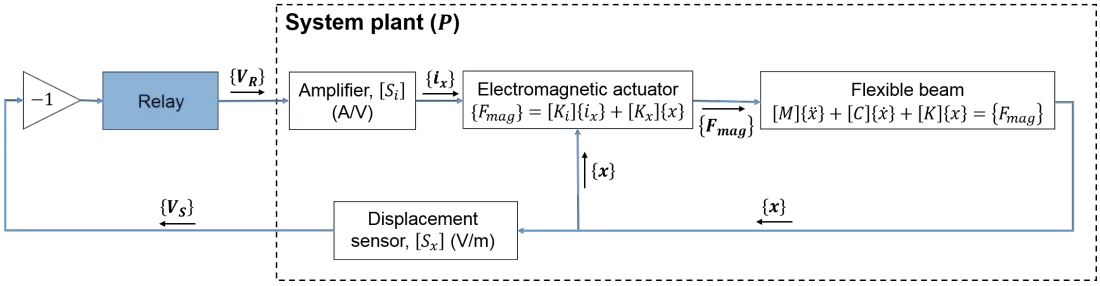

Figure 8 – Representation of the closed loop composed by the plant and the relay.

According to Anantachaisilp *et al*. (2012), "the goal of this test [the *relay feedback test*] is to determine the gain and the period as the magnitude of the relay is increased to the point where system becomes unstable (ultimate point)" (p. 6). The relay has also another parameter to be adjusted: the relay switch (the percentage of the pre-defined output signal that the input signal has to reach to switch the relay). Figure 9 shows an empirical application of the *relay feedback test*.

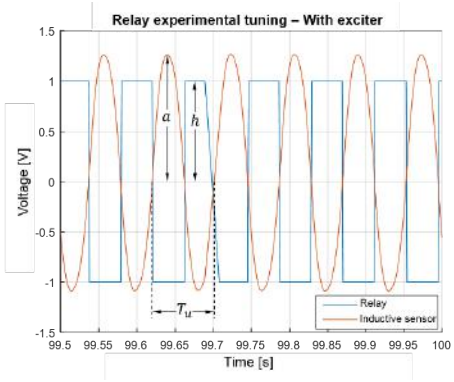

Figure 9 – Result of the *relay feedback test* obtained in the test rig.

In Fig. 9, T_u is the ultimate period of the output signal at the steady state of the test (ultimate period of the closed loop response). a is the amplitude of the plant output and h is the amplitude of the relay output. With a and h, it is possible to estimate de ultimate gain, K_u.

$$K_u = \frac{4h}{\pi a} \tag{7}$$

Again, the *relay feedback test* had to be applied twice: one for each case of excitation (once the mass load of the exciter changed the dynamics of the analyzed system). Tables 3 and 4 illustrates the concordance between the ultimate gain and ultimate period obtained either by simulation, either by the physical system in both cases of excitation. It must be noticed that the differences in the relay parameters from the simulated case to the experimental one may be attributed to inherent imperfections of the components in the physical system and in the measure equipment. Besides, although these differences in relay parameters, the relay itself does not compose the analyzed system. Therefore, its parameters cannot

change the system whose dynamic response is being investigated.

Table 3 – Results for the *relay feedback test* with shaker.

Parameters	Model	Experiment
Relay amplitude (V)	0.3	1.0
Relay switch (%)	0.5	5.0
Ultimate gain, K_u	1.0619	1.0825
Ultimate period, T_u	0.0844	0.0840

Table 4 – Results for the *relay feedback test* without shaker.

Parameters	Model	Experiment
Relay amplitude (V)	1.0	1.0
Relay switch (%)	5.0	0.8
Ultimate gain, K_u	1.3558	1.3234
Ultimate period, T_u	0.0295	0.0300

PID controller

Once the ultimate gain and ultimate period had been determined with the *relay feedback test*, the PID controller could be tuned. In this paper, following the example of Anantachaisilp *et al.* (2012), five different PID tuning methods were examined:

1. Ziegler-Nichols (ZN) method: a classic and fundamental PID tuning method, characterized, in general, by aggressive controllers, with fast response and high overshoots;
2. Ziegler-Nichols modified method for Some-Overshoot (SO-OV): modification of the ZN method to reduce the classical overshoot (reduced proportional gain of the PID);
3. Ziegler-Nichols modified method for No-Overshoot (NO-OV): modification of the ZN method to allow no overshoot (proportional gain reduced a little more);
4. Tyreus-Luyben (TL) method: an interesting method whose objective is to improve the robustness of the controller;
5. Shinskey (SH) method: another modification of the ZN method, whose objective is also to be less aggressive.

Table 5 summarizes the formulae for obtainment of the parameters of the PID controllers (for each tuning method) from the ultimate gain and the ultimate period of the closed loop.

Table 5 – Summary of PID tuning methods.

Method	K_P	T_I	T_D
ZN	0.60 K_u	0.50 T_u	0.125 T_u
SO-OV	0.33 K_u	0.50 T_u	0.330 T_u
NO-OV	0.20 K_u	0.50 T_u	0.330 T_u
TL	0.46 K_u	2.20 T_u	0.159 T_u
SH	0.25 K_u	0.50 T_u	0.120 T_u

In Tab. 5, K_P is the proportional gain of the PID controller; while T_I and T_D are the time constants, respectively, of the integral and derivative terms. From these parameters, the integral gain, K_I, and the derivative gain, K_D, can be obtained.

$$K_I = \frac{K_P}{T_I} \tag{8}$$

$$K_D = K_P T_D \tag{9}$$

The transfer function for the PID controller, considering a derivative filter (with coefficient N), would be:

$$TF := \frac{V_C}{V_S} = K_P + \frac{K_I}{s} + N\frac{K_D s}{N+s} \tag{10}$$

In Eq. 10, V_C is the output of the controller and V_S is the output of the inductive displacement sensor (input for the controller).

RESULTS

To analyze and guarantee the efficiency of the tuning methods, three complementary conditions of excitation were applied to the beam: first, the exciter generated a sinusoidal excitation at the natural bending frequencies of the beam; second, an impact hammer with steel tip applied impulsive excitations; and third, the shaker excited the structure randomly through white noise. Figure 10 illustrates the test rig assembly used to examine the efficiency of the different tunings.

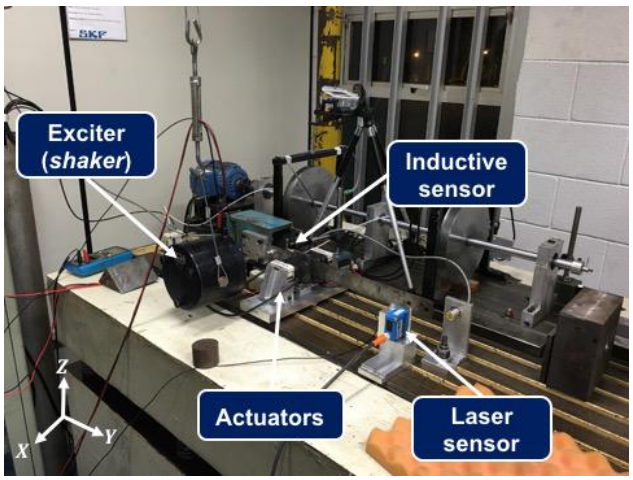

Figure 10 – Assembly of the test rig.

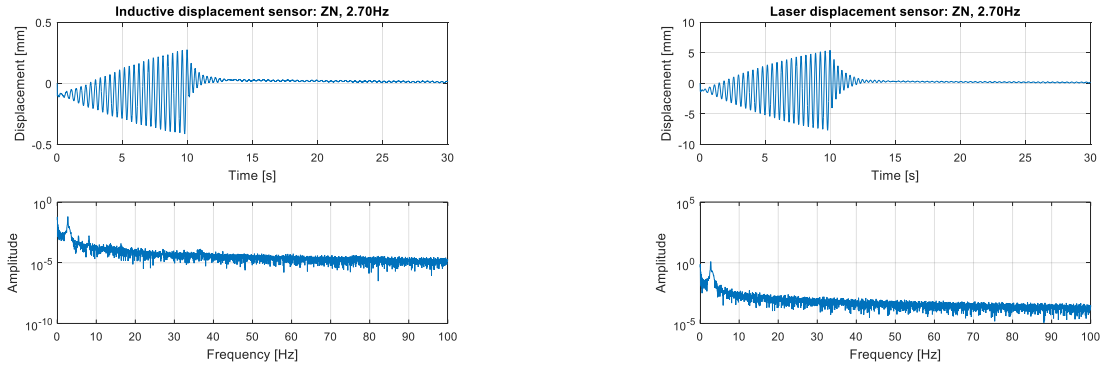

(a) Inductive sensor. **(b) Laser sensor.**

Figure 11 – Beam temporal response to excitation at 2.70Hz. Tuning method: ZN.

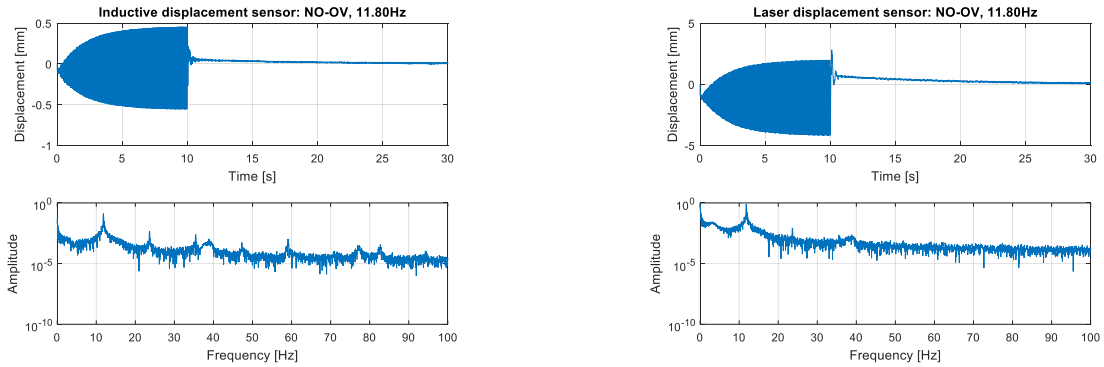

(a) Inductive sensor. **(b) Laser sensor.**

Figure 12 – Beam temporal response to excitation at 11.80Hz. Tuning method: NO-OV.

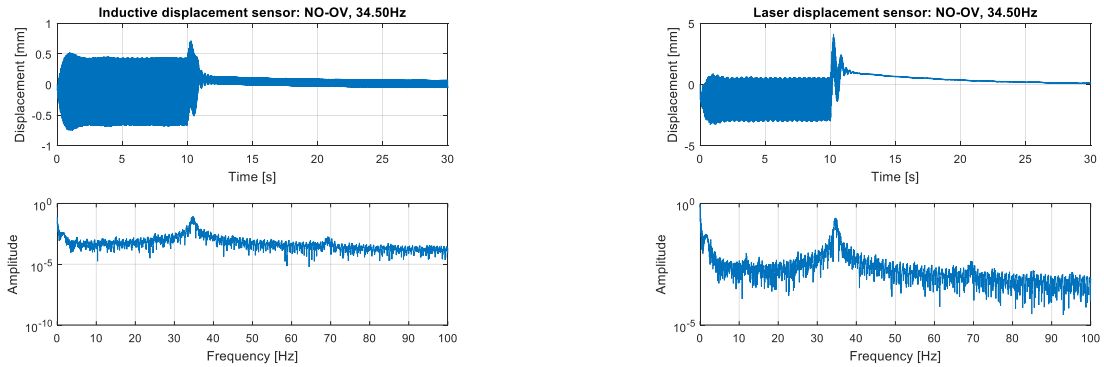

(a) Inductive sensor. **(b) Laser sensor.**

Figure 13 – Beam temporal response to excitation at 34.50Hz. Tuning method: NO-OV.

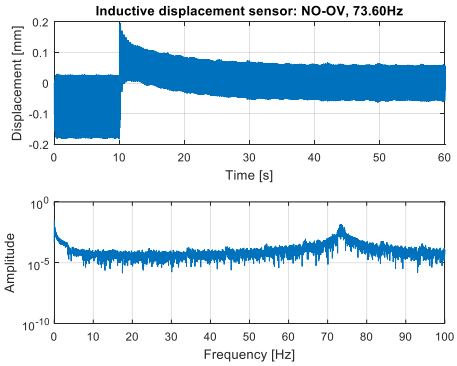

(a) Inductive sensor.

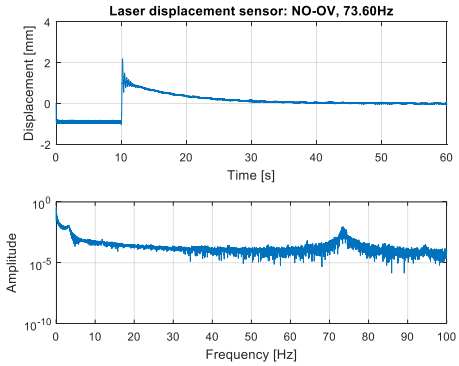

(b) Laser sensor.

Figure 14 – Beam temporal response to excitation at 73.60Hz. Tuning method: NO-OV.

Figures 11-14 shows the efficiency of the best tune for each natural frequency in damping the dynamic response of the beam in both displacement sensors. The beam was let free to vibrate during the first 10 seconds of each round, and then the controller started acting. The FFTs in Figures 11-14 aim only to show the excitation frequencies in each case.

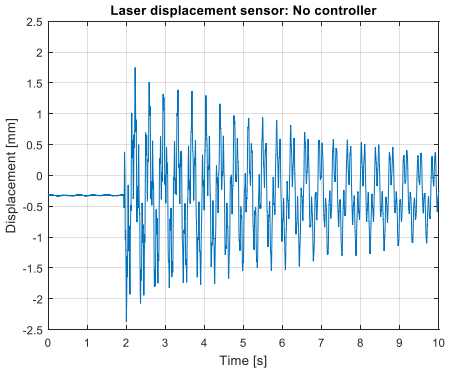

(a) No controller.

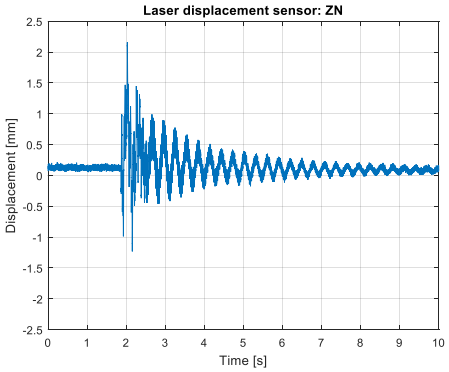

(b) ZN tuning.

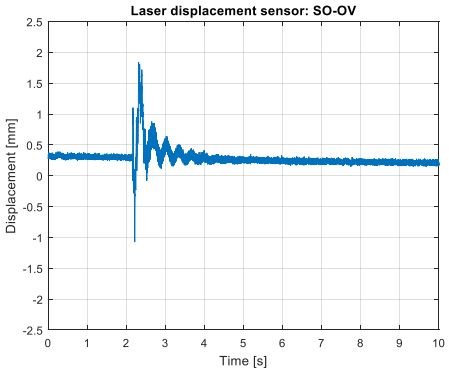

(c) SO-OV tuning.

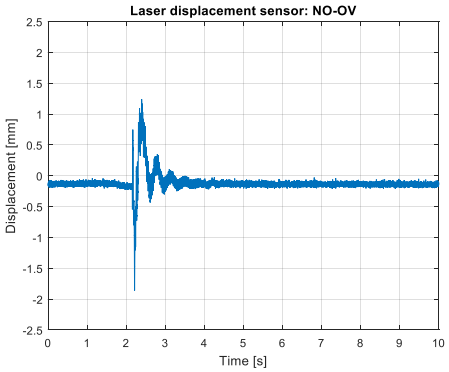

(d) NO-OV tuning.

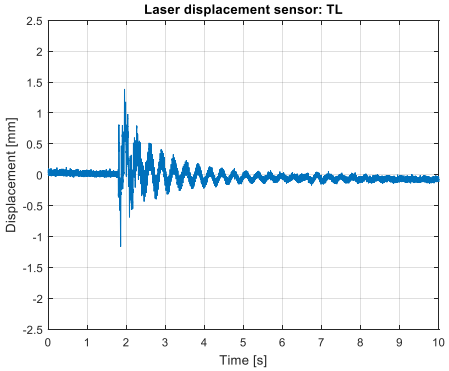

(e) TL tuning.

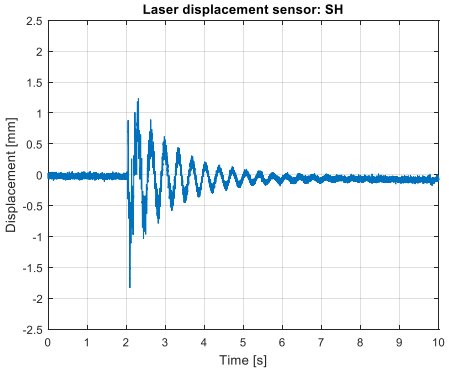

(f) SH tuning.

Figure 15 – Vibration of the beam due to an impact acquired with the laser sensor. Different tuning methods.

Figure 15 compares directly the efficiency of the different tuning methods in accelerating the decay of the transient regime (damping increasing) of the beam dynamic response to an impulsive excitation.

Finally, Fig. 16 presents the frequency response functions of the beam excited randomly with white noise. The data were acquired with both displacement transducers (inductive and laser) and still with an accelerometer near the mid-point of the beam free length.

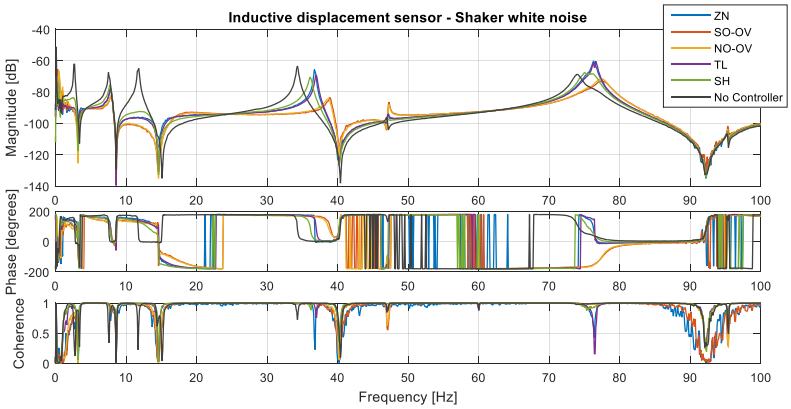

(a) Inductive displacement sensor feeding the controller.

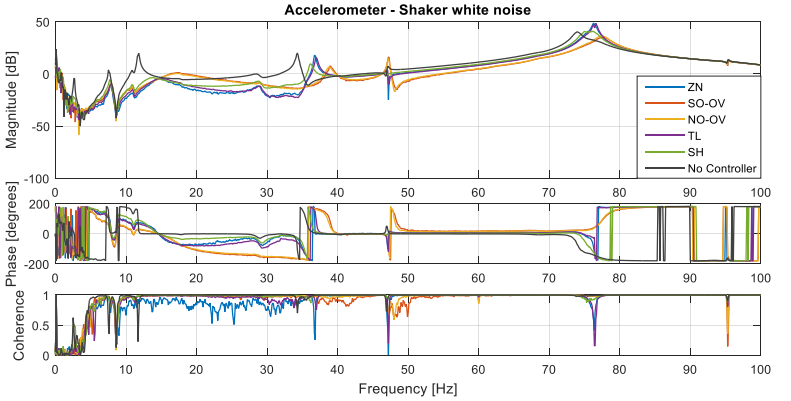

(b) Accelerometer near the center of the free length of the beam.

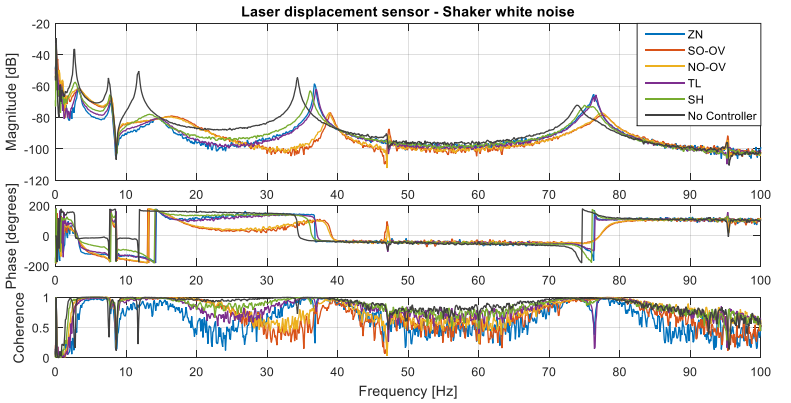

(c) Laser displacement sensor near the free extremity of the beam.

Figure 16 – FRFs of the cantilever beam with journal and exciter coupled. Different tuning methods.

CONCLUSIONS

The tests proved the efficiency of the different tuning methods of the PID controller. All of them could attenuate the vibration amplitude of motion of the beam, at the steady state regime, for both the sinusoidal and impact excitation. Besides, Fig. 15 illustrates the effect of the control force over the beam dynamics: the system controlled is more damped. Therefore, its response presents a faster decay when compared to that from the same system without control. Figure 15 illustrates still that some tuning methods resulted in more efficient controllers (such as the Zigler-Nichols modifications

Some-Overshoot, SO-OV, and *No-Overshoot*, NO-OV).

From Figs. 11-14 one must notice the dual mechanism of acting of the controller: along with the attenuation of the amplitude of motion, the control system could keep the beam at its reference position. It must be noticed too (specially from Fig. 12) that even when the system response occurred in more than one frequency, the controller was capable of acting efficiently.

Finally, Fig. 16 synthesizes previous results. It shows the expressive amplitude reduction from the system with any of the tuned controllers with respect to the non-controlled system (specially at lower natural frequencies). Figure 16 also demonstrates that the efficiency of the controller system is felt by the entire beam, by its entire free length, once the inductive sensor is near the clamped portion of the beam, and the laser sensor is near its free extremity (with the accelerometer somewhere between those sensors). It must be noticed too, from Fig. 16, that as the frequency grows, the efficiency of the tuning methods reduces progressively. At the fourth bending natural frequency (73.60Hz), only the tunings SO-OV and NO-OV remain capable of controlling the dynamics of the system.

Quantitatively, some tunings, at some natural frequencies, were able to reduce almost 99% of the non-controlled amplitude of the system at the inductive sensor and almost 97% at the laser sensor. Higher frequencies (above 100Hz) were not tested because the controller system efficiency was almost completely lost by those frequencies.

ACKNOWLEDGMENTS

The authors would like to thank Professor Robson Pederiva and Marcos Vieira de Albuquerque for their precious contribution to this work. Also, the authors thank CNPq Grant # 406234/2013-2 and CAPES for funding this research.

REFERENCES

Anantachaisilp, P., Lin, Z., Allaire, P, 2012, PID Tuning Methods for Active Magnetic Bearing Systems, 13th International Symposium on Magnetic Bearings, Arlington, VA, USA.

ASTM E 1876-09, Dynamic Young's Modulus, Shear Modulus, and Poisson's Ratio by Impulse Excitation of Vibration, 2009.

Åström, K. J., Hägglund, T. PID Controllers: Theory, Design, and Tuning, 1994. 343pp.

Friswell, M. I., Penny, J. E. T., Garvey, S.D., 2000, Model Reduction for Structures with Damping and Gyroscopic Effects, ISMA 25, Leuven, Belgium, p. 1151-1158.

Guyan, R. J, 1965, Reduction of stiffness and mass matrices, AIAA Journal, Vol. 3, No. 2, p. 380.

Kwon, Y. W. The finite element method using MATLAB. CRC Press, 1996. 519 p.

Maia, N. M. M., and Silva, J. M. M. Theoretical and experimental modal analysis. RSP, 1997. 468p.

Maslen, E. Magnetic Bearings. University of Virginia, 2000. 231p.

RESPONSIBILITY NOTICE

The authors are the only responsible for the material included in this paper.